Variability of the cold season climate in central asia. Part II: Hydroclimatic predictability

Lars Gerlitz, Eva Steirou, Christoph Schneider, Vincent Moron, Sergiy Vorogushyn, Bruno Merz

Variability of the Cold Season Climate in Central Asia. Part II: Hydroclimatic Predictability⌗

LARS GERLITZ AND EVA STEIROU

Hydrology Section, GFZ German Research Centre for Geosciences, Potsdam, Germany

CHRISTOPH SCHNEIDER

Institute of Geography, Humboldt-Universität zu Berlin, Berlin, Germany

VINCENT MORON

Aix-Marseille University, CNRS, IRD, INRA, Coll. de France, CERFGE, Aix-en-Provence, France

SERGIY VOROGUSHYN

Hydrology Section, GFZ German Research Centre for Geosciences, Potsdam, Germany

BRUNO MERZ

Hydrology Section, GFZ German Research Centre for Geosciences, and Institute of Environmental Sciences and Geography, Universität Potsdam, Potsdam, Germany

ABSTRACT

Central Asia (CA) is subjected to a large variability of precipitation. This study presents a statistical model, relating precipitation anomalies in three subregions of CA in the cold season (November–March) with various predictors in the preceding October. Promising forecast skill is achieved for two subregions covering 1) Uzbekistan, Turkmenistan, Kyrgyzstan, Tajikistan, and southern Kazakhstan and 2) Iran, Afghanistan, and Pakistan. ENSO in October is identified as the major predictor. Eurasian snow cover and the quasi-biennial oscillation further improve the forecast performance. To understand the physical mechanisms, an analysis of teleconnections between these predictors and the wintertime circulation over CA is conducted. The correlation analysis of predictors and large-scale circulation indices suggests a seasonal persistence of tropical circulation modes and a dynamical forcing of the westerly circulation by snow cover variations over Eurasia. An EOF analysis of pressure and humidity patterns allows separating the circulation variability over CA into westerly and tropical modes and confirms that the identified predictors affect the respective circulation characteristics. Based on the previously established weather type classification for CA, the predictors are investigated with regard to their effect on the regional circulation. The results suggest a modification of the Hadley cell due to ENSO variations, with enhanced moisture supply from the Arabian Gulf during El Niño. They further indicate an influence of Eurasian snow cover on the wintertime Arctic Oscillation (AO) and Northern Hemispheric Rossby wave tracks. Positive anomalies favor weather types associated with dry conditions, while negative anomalies promote the formation of a quasi-stationary trough over CA, which typically occurs during positive AO conditions.

1. Introduction

With its continental climate, central Asia (CA) is characterized by water scarcity and a pronounced variability of precipitation. While the summer is usually dry, a significant portion of the annual precipitation falls

during the extended winter season (from November to March, hereafter called the cold season) (Schiemann et al. 2008; Barlow et al. 2016). Particularly in the high Tien Shan and Pamir mountain regions precipitation falls as snow and is released during spring and summer, when it is required for irrigated agriculture, particularly in Uzbekistan and Kazakhstan, where cotton and wheat production represent an important source of income. The upstream countries Kyrgyzstan and Tajikistan additionally need the water for hydropower production. Thus the variability of the cold season precipitation poses challenges to the post-Soviet economies and raises political tensions. The prolonged drought of 1999–2001 as well as the drought event of 2007/08 had far-reaching consequences, such as regionwide crop failure, loss of livestock, breakdown of hydropower electricity production, and an increase in diseases (Barlow et al. 2016). Likewise, climate-induced refugee movements and international conflicts on water allocation and management have been reported (Lautze et al. 2002; Barlow et al. 2016; Agrawala et al. 2001).

A robust seasonal forecast of summer water availability is required in order to adapt the agricultural strategies to anomalous hydroclimatic conditions and to allow a fair water distribution between the central Asian countries and thus to prevent potential political conflicts. Some forecast skill has been achieved by means of simple statistical techniques, taking cold season precipitation or remote sensing–based estimates of the regional snow cover extent in spring as predictor variables for summer discharge in several central Asian river basins (Schär et al. 2004; Dixon and Wilby 2016; Barlow and Tippett 2008; Apel et al. 2018). However, the significant predictors do not emerge before late spring and thus enable a forecast of summer runoff anomalies only a few months in advance. A profound understanding of cold season hydroclimatic variations, associated large-scale atmospheric processes, and their driving mechanisms is crucial in order to extend the lead time of seasonal predictions of water availability.

In Part I of the presented study (Gerlitz et al. 2018, hereafter Part I) we comprehensively analyzed the variability of the cold season climate in central Asia by means of an automatic weather classification approach. Eight weather types (WTs) were identified and investigated with regard to their tropical and extratropical drivers and their near-surface climate expression. Anomalously moist WTs were shown to be associated with the formation of a Rossby trough over central Asia, which triggers a southward shift of the westerly jet stream and an intensification of westerly moisture advection into the target domain. Particularly the superposition of the positive states of the North Atlantic

Oscillation (NAO) and the east Atlantic/western Russia pattern (EA/WR) has been shown to favor WTs associated with moist conditions. Besides westerly circulation modes, El Niño–Southern Oscillation (ENSO) has been shown to significantly influence the frequency of WTs characterized by strong pressure anomalies in the south of the target domain. El Niño events are shown to stimulate the formation of an anticyclonic circulation anomaly over the Indian subcontinent and thus the intensification of southwesterly moisture fluxes from the Arabian Sea into central Asia. This leads to increased precipitation amounts during the ENSO warm phase.

As ENSO is characterized by a low-frequency variability and usually shows a seasonally persistent behavior, ENSO indices have been suggested as skillful predictor variables for seasonal climate forecasts. Precipitation predictions in tropical regions are frequently based on ENSO variations (Kumar et al. 2013), but ENSO-related indices have also been suggested as skillful predictors of seasonal precipitation in various extratropical regions. For central and Southwest Asia, variations of tropical circulation modes, such as ENSO and the Indo-Pacific warm pool (which is strongly anticorrelated with ENSO), have been suggested as important drivers of precipitation variations and changes (Gerlitz et al. 2016; Mariotti 2007; Barlow et al. 2002, 2016; Roghani et al. 2016). However, because of the dominant influence of westerly wave tracks, their embedded synoptic features, and associated moisture fluxes, the skill of statistically based seasonal precipitation forecast models is generally low in extratropical regions. Although several studies highlight the importance of Eurasian Rossby wave tracks for the central Asian winter climate (Part I; Bothe et al. 2012; Syed et al. 2006; Schiemann et al. 2008), little effort has yet been made to predict anomalous westerly moisture fluxes and related hydroclimatic variations in central Asia.

Notwithstanding, various studies investigate the predictability of the large-scale Eurasian winter climate, particularly with regard to variations of the Arctic Oscillation (AO) and NAO. Auspicious progress has been made by considering snow cover anomalies in October as a predictor variable for the mean state of the Arctic Oscillation during subsequent winter (Cohen and Entekhabi 1999; Cohen et al. 2012). Both observational and modeling studies indicate that enhanced snow cover over Eurasia in October triggers an early and strong formation of the Siberian high due to an increased surface albedo and a consequential diabatic cooling and stabilization of the planetary boundary layer (Cohen 1994; Gastineau et al. 2017). The resultant increase of the zonal pressure gradient between the eastern Arctic

and the northern Eurasian continent provokes the formation of a persistent wave pattern that propagates into the upper troposphere and leads to a weakened stratospheric polar vortex (Cohen et al. 2014). Particularly in December and January, a significantly increased frequency of weak polar vortex conditions has been observed after positive snow cover and sea level pressure anomalies over Siberia (Kretschmer et al. 2016). A subsequent downward propagation of wave activity promotes the development of a negative AO and the occurrence of cold air outbreaks in the midlatitudes. On the contrary, reduced snow cover over Eurasia triggers a strong zonal flow and favors positive AO conditions. Allen and Zender (2011) show that a positive trend of the winter AO index for the period 1950–90 and a negative trend thereafter are closely related to decadal variations of autumn snow cover over Eurasia.

Cohen and Jones (2011) illustrate that Eurasian snow cover in October serves as a skillful covariate for the prediction of winter temperature for large parts of the Northern Hemisphere. García-Serrano and Frankignoul (2014), Brands et al. (2012), and Totz et al. (2017) demonstrate the potential of statistically based winter precipitation forecasts for Europe taking cryospheric variables (i.e., snow cover and sea ice) over Eurasia and the Arctic during preceding autumn as covariates. Further, SST anomalies in the Atlantic domain (most notably the Atlantic tripole) have been suggested as potential drivers of AO/NAO (Sutton et al. 2000; Czaja and Frankignoul 2002; Cassou et al. 2004). Finally, the quasi-biennial oscillation (QBO), a dominant and well predictable mode of variability in the tropical stratosphere has been identified as a potential predictor for the winter state of AO/NAO (Boer and Hamilton 2008; Marshall and Scaife 2009; Scaife et al. 2014). Observations show that the positive phase of QBO (corresponding to westerly winds in the tropical stratosphere) is associated with a stronger and zonally oriented polar vortex, which favors the development of a positive AO. Negative correlations between the QBO index and sea level pressure during winter have been detected for large parts of Eurasia, including CA (Boer and Hamilton 2008).

Here we intend to quantify the skill of various predictors, including Euro/Atlantic pressure modes, tropical SST anomalies, and Eurasian snow cover indices in October, for the forecast of cold season precipitation anomalies in CA. A multilinear regression-based seasonal forecast model with stepwise predictor selection is presented and applied to three subregions of the target domain, which are previously derived by means of a cluster analysis of interannual precipitation variations. The investigation of teleconnections based on the statistical relation of large-scale climate indices with surface variables, however, is associated with large uncertainties, due to the quality and the short period of available observations, which often results in a lack of statistical significance and might lead to spurious correlations. To bridge the scale gap between large-scale teleconnection indices and observed precipitation anomalies, we analyze the influence of the identified predictor variables on the large- and regional-scale circulation over CA. To quantify the effect of important predictor variables at the Northern Hemispheric scale, predictors are related with seasonal mean climate indices in the subsequent cold season. An empirical orthogonal function (EOF) analysis of pressure and humidity fields is conducted to distinguish the major circulation modes over CA. The separation of westerly and tropical circulation modes enables the assignment of particular predictor variables to the respective portion of the atmospheric variability.

Finally, based on the previously established objective WT classification (Part I), we investigate the influence of the identified predictor variables on the synoptic regimes and the regional-scale circulation. WTs are analyzed with regard to their pressure patterns and moisture fluxes and the consequential precipitation characteristics. The major predictor variables of the regression model (particularly ENSO and Eurasian snow cover) are related to the frequency of WTs in the subsequent cold season, which allows assessing the influence of tropical and extratropical drivers on the regional circulation over CA and the associated precipitation climate. Section 2 gives a brief overview of the data and the applied statistical techniques. In section 3 the skill of the statistical model is discussed and the effects of the identified predictor variables on the large and regional-scale circulation over central Asia are investigated in detail. Section 4 summarizes the findings and discusses the applicability of the results.

2. Data and methods

The operational model is based on the free and open source programming interface of R (R Development Core Team 2008) and makes use of freely available datasets only, which are automatically downloaded and processed.

a. Precipitation data and preprocessing

Various precipitation datasets are available covering CA, including gridded observations such as CRU-TS (Harris et al. 2014; New et al. 1999), APHRODITE (Yatagai et al. 2012), and GPCP (Adler et al. 2003), and reanalysis data such as ERA-Interim (Dee et al. 2011),

ERA-Interim/Land (Balsamo et al. 2015), and NCEP–NCAR (Kalnay et al. 1996). Most of the datasets are in close agreement concerning the variability of cold seasonal precipitation sums (not shown). The presented study is based on the ERA-Interim reanalysis, which provides 6-hourly surface climate estimates as well as large-scale atmospheric fields for 60 pressure levels between 1000 and 1 hPa at a spatial resolution of 0.75°. The reanalysis spans the period after 1979 and is continuously extended, which allows a regular recalibration and re-evaluation of the forecasting model. Since ERA-Interim combines modeling results with ground and radiosonde observations and remote sensing data using a 4D data assimilation system, the free-atmosphere fields can be considered as the best guess of large-scale atmospheric conditions. Several studies show that ERA-Interim sufficiently simulates the variability of relevant free-air and near-surface meteorological parameters, even over the complex mountain regions of central and High Asia (Bao and Zhang 2013; Gao et al. 2014; Wang and Zeng 2012; Liu et al. 2018).

Precipitation estimates are obtained for a domain covering the entire CA (50°–80°E, 30°–55°N). The precipitation fields are aggregated to cold seasonal sums (November–March) and converted to the standardized precipitation index (SPI) for each grid cell (Guttman 1998). For this purpose, a gamma distribution is fitted to the empirical distribution of precipitation and the exceedance probability of observed precipitation sums is converted to z scores of the normal distribution. The gridded SPI time series are aggregated to regions with quasi-homogeneous precipitation variability by means of a bootstrap clustering approach (Hennig 2007). For a predefined range of cluster numbers ($k = 1$–8), a k-means clustering is conducted with the original SPI time series and with 100 artificial records, derived by means of bootstrap resampling. The robustness of the clustering results is estimated for each cluster of a partition with k elements based on the Jaccard coefficient J. Values of $J > 0.75$ suggest robust clusters, whereas values of $J < 0.5$ indicate a high uncertainty of the cluster solution (Hennig 2007). To select a robust but still detailed partition, the adequate number of quasi-homogeneous regions is chosen as the maximum k with $J > 0.75$ for all clusters. The SPI time series are spatially averaged for each cluster region and spatial mean SPI values serve as predictand variables for the forecasting model.

b. Predictor selection, model calibration, and evaluation

The mean cold seasonal precipitation anomalies in each region are analyzed with regard to their statistical relationships with various predictor variables in preceding October. A comprehensive list of potential predictor variables, with their abbreviations and definitions, is given in Table 1. Possible mechanisms are suggested based on the introductory literature review and marked with W indicating a potential influence on westerly moisture fluxes and T indicating a potential influence on tropical moisture fluxes. The Euro/Atlantic pressure modes (AO, NAO, EA, EA/WR, SCA, POL/EUR; see Table 1) as well as most of the SST indices (ATP, Niño-1+2, Niño-3.4, Niño-4, AMO, PDO, WHWP; see Table 1) and tropical circulation modes (SOI, QBO; see Table 1) are available for download from the National Oceanic and Atmospheric Administration (www.esrl.noaa.gov/psd/data). The monthly mean SSTs of the Indo-Pacific warm pool (WP; 10°S–10°N, 120°–150°E) are extracted from the global ERSST v03 dataset (Smith and Reynolds 2003). Snow-related parameters [Eurasian snow cover (SC), Europe SC, Siberia SC, High Asia SC, and snow advance index (SAI); see Table 1] are derived from the Northern Hemispheric Snow Cover Extent (NH-SCE) dataset (Estilow et al. 2015), which provides weekly gridded snow cover maps since 1971 based on various sources of satellite imagery and in situ observations. The snow cover extent is extracted for all of Eurasia as well as for Europe (20°W–50°E, 30°–70°N), Siberia (60°–180°E, 50°–80°N), and High Asia (60°–110°E, 20°–50°N) and the maximum snow coverage in October is derived. The SAI (Brands et al. 2012), defined as the linear increase of snow cover over Eurasia during October, is calculated as the linear regression of four weekly snow cover estimates. All predictor variables are normalized by mean and standard deviation.

A multiple linear regression model is separately established for each subregion based on a stepwise procedure, including forward selection and backward elimination of predictor variables (von Storch and Zwiers 2002; Hertig and Jacobeit 2011). Starting with the predictor, which is most significantly correlated with the SPI time series, the iterative procedure includes one additional covariate at each step, as long as additional variables are found to significantly improve the regression results (F test; $\alpha = 0.1$). To avoid the selection of predictor variables that are only correlated with observed precipitation sums due to a common temporal trend, the predictor selection procedure is conducted for detrended time series. The regression model is developed based on all selected predictor variables by means of the least squares fit and utilized the original nondetrended records. The statistical model is cross-validated by a leave-one-out procedure; that is, at each step of the cross-validation one year is omitted and

TABLE 1. Potential predictors for the linear precipitation forecast model; W indicates a potential influence on westerly moisture fluxes and T a potential influence on tropical moisture fluxes.

Abbreviation	Definition	Source	Potential mechanism
AO	Arctic Oscillation	NOAA	W
NAO	North Atlantic Oscillation	NOAA	W
EA	East Atlantic pattern	NOAA	W
EA/WR	East Atlantic/western Russia pattern	NOAA	W
SCA	Scandinavian pattern	NOAA	W
POL/EUR	Polar/Eurasian pattern	NOAA	W
ATP	Atlantic SST tripole	NOAA	W
Niño-1+2	Normalized SST in ENSO-12 region (0°–10°S, 90°–80°W)	NOAA	T
Niño-3.4	Normalized SST in ENSO-34 region (5°N–5°S, 170°–120°W)	NOAA	T
Niño-4	Normalized SST in ENSO-4 region (5°N–5°S, 160°E–150°W)	NOAA	T
TNI	Trans-Niño index, difference of Niño-1+2 and Niño-4	NOAA	T
AMO	Atlantic multidecadal oscillation	NOAA	W
QBO	Quasi-biennial oscillation	NOAA	W
PDO	Pacific decadal oscillation	NOAA	T
WHWP	Monthly anomaly of the ocean surface area warmer than 28.5°C in the Atlantic and eastern North Pacific	NOAA	T
WP	Normalized SST of Indo-Pacific warm pool (10°S–10°N, 110°–130°E)	ERSST v03	W/T
SAI	Snow advance index	NH-SCE	W
Eurasia SC	Snow cover anomalies over Eurasia	NH-SCE	W
Siberia SC	Snow cover anomalies over Siberia (60°–180°E, 50°–80°N)	NH-SCE	W
Europe SC	Snow cover anomalies over Europe (20°–50°E, 30°–70°N)	NH-SCE	W
High Asia SC	Snow cover anomalies over High Asia (60°–110°E, 20°–50°N)	NH-SCE	W

predictor selection and regression calibration are conducted based on the remaining data. Various regression models, which might be based on different predictor combinations, are generated during cross-validation. This allows quantifying the uncertainty arising from both the selection of covariates and the statistical fit. The skill of the model is specified as the correlation coefficient of observed and hindcasted SPI values for both the final regression model (considering all available years) and the cross-validation. A 90% prediction interval of the forecast is estimated by means of a residual-based approach, assuming that cross-validated model errors follow a normal distribution. The final model output displays the frequency of predictor selection during the cross-validation for each subregion. Further, normalized time series of the selected predictors and the fractional response of the final regression model are plotted. The fractional response of a particular predictor variable is calculated as the result of the regression model applied to a modified predictor time series, which retains the values of the considered covariate, while other covariates are set to zero. Finally the modeling

results, including observed, modeled, and cross-validated SPI time series and the 90% prediction interval, are presented for each subregion. For the operational precipitation forecast, the model only considers predictors, which are selected by more than 50% of the models during cross-validation.

c. Predictor influence on large- and regional-scale circulation patterns

To better understand the teleconnections and atmospheric mechanisms behind the skill of the statistical forecasting approach, the effect of the predictor variables on the central Asian climate is investigated at two different spatial scales: a large scale considering the state of Northern Hemispheric circulation and a regional one focusing on the prevalent synoptic patterns over central Asia. For a large-scale perspective, predictors are statistically related with mean circulation indices and ERA-Interim fields of geopotential height and humidity for the cold seasons 1979/80 to 2016/17. To distinguish the major modes of circulation variability affecting the target region, we conduct an EOF analysis of seasonal

(November–March) mean ERA-Interim 500-hPa geopotential height and total column water fields for a domain covering 0°–90°E, 20°–70°N. This domain covers the western part of the Eurasian continent as well as the Indian Ocean and thus includes the previously identified moisture sources of the central Asian winter climate (Part I; Syed et al. 2006; Mariotti 2007). Spatial loadings of pressure and humidity are analyzed for three dominant patterns and the time series of EOF scores are related to the contemporaneous state of large-scale circulation indices as well as to predictor variables in preceding October. Finally, focusing on regional synoptic patterns and associated precipitation anomalies, we analyze the previously established automatic WT classification for central Asia (for details on the classification methodology, see Part I). The influence of predictor variables in October on the frequency of dry and moist WTs during subsequent cold season is quantified by means of a univariate composite analysis. Data are divided into seasons representing a rather negative (0%–33% quantile), normal (33%–66%), and positive state (66%–100% quantile) of the considered predictor variable, and the mean seasonal WT frequency anomaly (%) is depicted. Statistically significant deviations (t test, $\alpha = 0.1$) from the overall frequency mean are highlighted and discussed with regard to their large-scale drivers.

3. Results

a. Seasonal precipitation forecast: Predictors and skill

Three quasi-homogeneous regions of cold season precipitation variability have been identified by the bootstrap cluster approach (Fig. 1). A Jaccard coefficient $J > 0.9$ suggests a robust partition of the data into three clusters. In contrast, values of $J < 0.7$ for cluster solutions with $k = 2$ or $k \geq 4$ indicate a considerably higher uncertainty and a rather fuzzy separation of the data (Fig. 1a). Subregion 1 covers the northern Kazakh plains and is bordered by the Kazakh uplands (Fig. 1b). Subregion 2 encompasses southern Kazakhstan, Uzbekistan, Kyrgyzstan, Tajikistan, and northern Turkmenistan and extends to the mountain barriers of Pamir and Elburz. Subregion 3 includes the territories of Iran, Afghanistan, and Pakistan. The SPI time series for regions 2 and 3 (Fig. 1d) clearly exhibit the central Asian droughts of 1999–2001 and 2007/08. The correlations between SPI time series of different cluster region appear to be insignificant for the period 1979–2017 (Fig. 1c).

A correlation analysis of all predictor variables with observed SPI time series in each subregion (Fig. 1e) indicates a strong influence of ENSO-related variables

for regions 2 and 3. Correlations exceed $r = 0.4$ and are highly significant. This also applies to PDO and WP, which are strongly correlated with ENSO (see Fig. S1 in the online supplemental material for the cross-correlation matrix of all predictor variables). Significant correlations of cold season precipitation in regions 2 and 3 are also detected for October NAO; however, a high correlation between NAO/AO and ENSO indices in October has also been observed (see the online supplemental material). This can either be coincidental or indicate a coupling between NAO and ENSO due to an effect of extratropical Pacific SSTs on Northern Hemispheric planetary wave tracks, as reported by Wu and Lin (2012). Positive correlations with October QBO are detected for all regions, but are only statistically significant for region 3. Further, negative correlations of snow related predictors (Eurasian, Siberian, and High Asian snow cover) are distinctly defined for regions 2 and 3, although not always significant. The SPI time series of region 1 is characterized by an absence of significant correlations with large-scale predictor variables, indicating that a robust forecast of seasonal precipitation by means of the linear regression approach is rather unfeasible for the northern Kazakh plains. In general, cold season precipitation sums over the northern Kazakh plains are low (<200 mm) and single, nonpredictable precipitation events may significantly affect the SPI time series. No model development was thus carried out for region 1. In contrast, regions 2 and 3 are characterized by high mountain terrain resulting in a frequent uplift of westerly and tropical air masses. This leads to considerably higher precipitation amounts (up to 800 mm during cold season at west facing slopes) and also to a stronger influence of large-scale atmospheric variations.

Modeling results for regions 2 and 3 are presented in Fig. 2. The cross-validated correlations between observations and predictions for regions 2 and 3 amount to 0.34 and 0.41, respectively, which is a similar skill compared with more complex and nonlinear statistical forecasting models for central Asia (see, e.g., Gerlitz et al. 2016). Although the prediction range is large (with SPI ± 1.0 for region 2 and SPI ± 1.3 for region 3), the major characteristics of interannual precipitation variability are well captured for both regions. Both time series feature drought events in 1985/86, 1999–2001, and 2007/08, which are also apparent in the hindcast modeling results. The same applies for an additional drought in region 3 in 1997 and a period of primarily positive SPI anomalies in both regions during the early 1990s.

The Niño-4 index is identified as an important predictor for both regions. Siberian snow cover and the Scandinavian pattern are selected as secondary
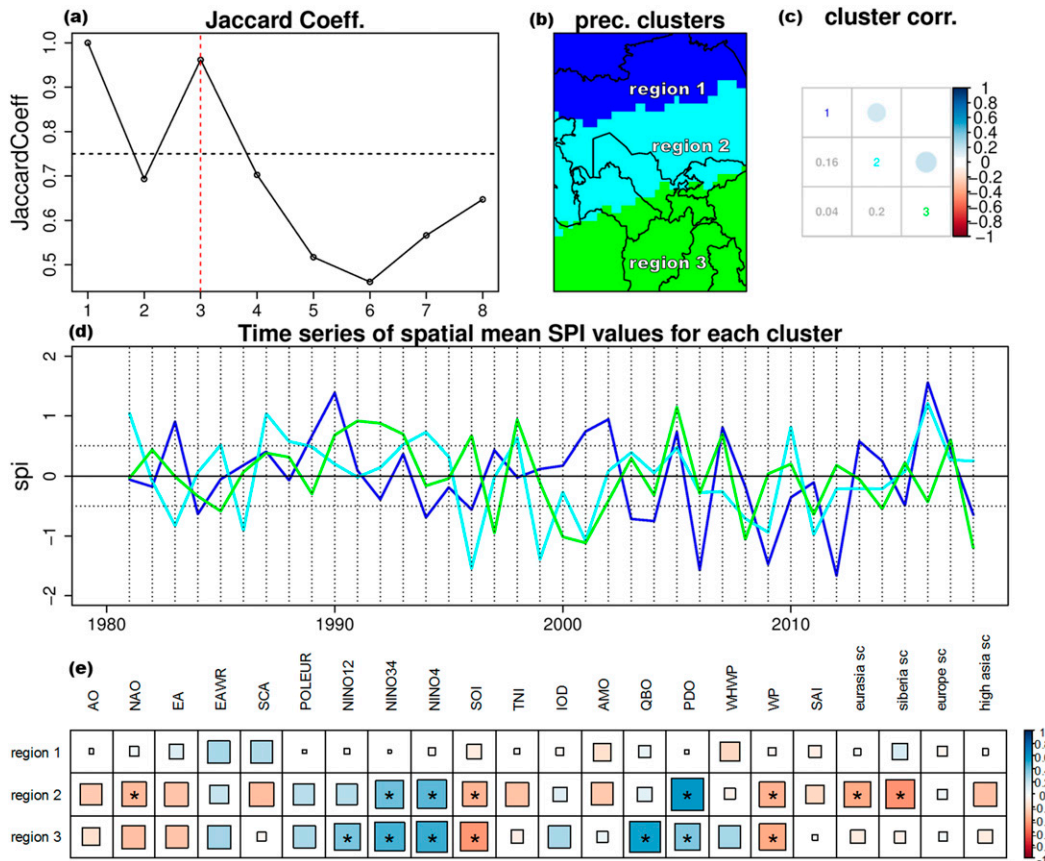
FIG. 1. Clustering results of cold seasonal SPI variations over central Asia. (a) Minimum Jaccard coefficient for cluster solutions with $k = 1$–8 clusters. (b) Quasi-homogeneous regions of precipitation variability over central Asia, based on a cluster solution with $k = 3$. (c) Pearson correlations of the mean SPI time series for three subregions. The size of circles is proportional to the correlation values. (d) Time series of mean SPI values for each cluster region. (e) Pearson correlations of mean cold seasonal SPI for each region with potential predictor variables in the preceding October. The size of squares is proportional to the correlation values. Significant correlations ($\alpha = 0.1$) are marked with an asterisk (*).

covariates for cluster 2. For cluster 3 the quasi-biennial oscillation and SCA are considered as further predictors. The analysis of various linear models generated during the cross-validation procedure indicates a robust predictor selection (Fig. 3). More than 80% of the models are based on the aforementioned predictor combinations. Occasionally, Niño-4 is replaced by other ENSO-related covariates (Niño-3.4, IOD) and Siberian snow cover is substituted by other snow indices. Notably, some models also select snow cover–related predictor variables for region 3. Because of a strong intercorrelation of snow cover indices (Fig. S1), an independent analysis of the impact of snow cover anomalies in different subregions of Eurasia based on statistical techniques appears to be difficult. The same applies for ENSO-related covariates.

The time series of predictor variables and the fractional predictor response of the linear model indicate

that drought events are mainly associated with the negative (cold) phase of ENSO. The positive response of the regression model for region 3 to variations of QBO is particularly evident during the 2000s, where SPI anomalies appear to be characterized by a biannual cycle. A negative response to variations of the Scandinavian pattern is apparent for both regions. For region 2, a negative influence of snow cover–related predictor variables is clearly depicted. Siberian snow cover is characterized by mainly negative anomalies before 1995 and positive anomalies thereafter, which leads to a positive response of the regression model until the mid-1990s and a subsequent negative feedback. The SPI time series for both regions show slight, although not statistically significant, negative trends (Part I), indicating that Eurasian snow cover should be considered as a potential driver of the drying tendency during recent decades.
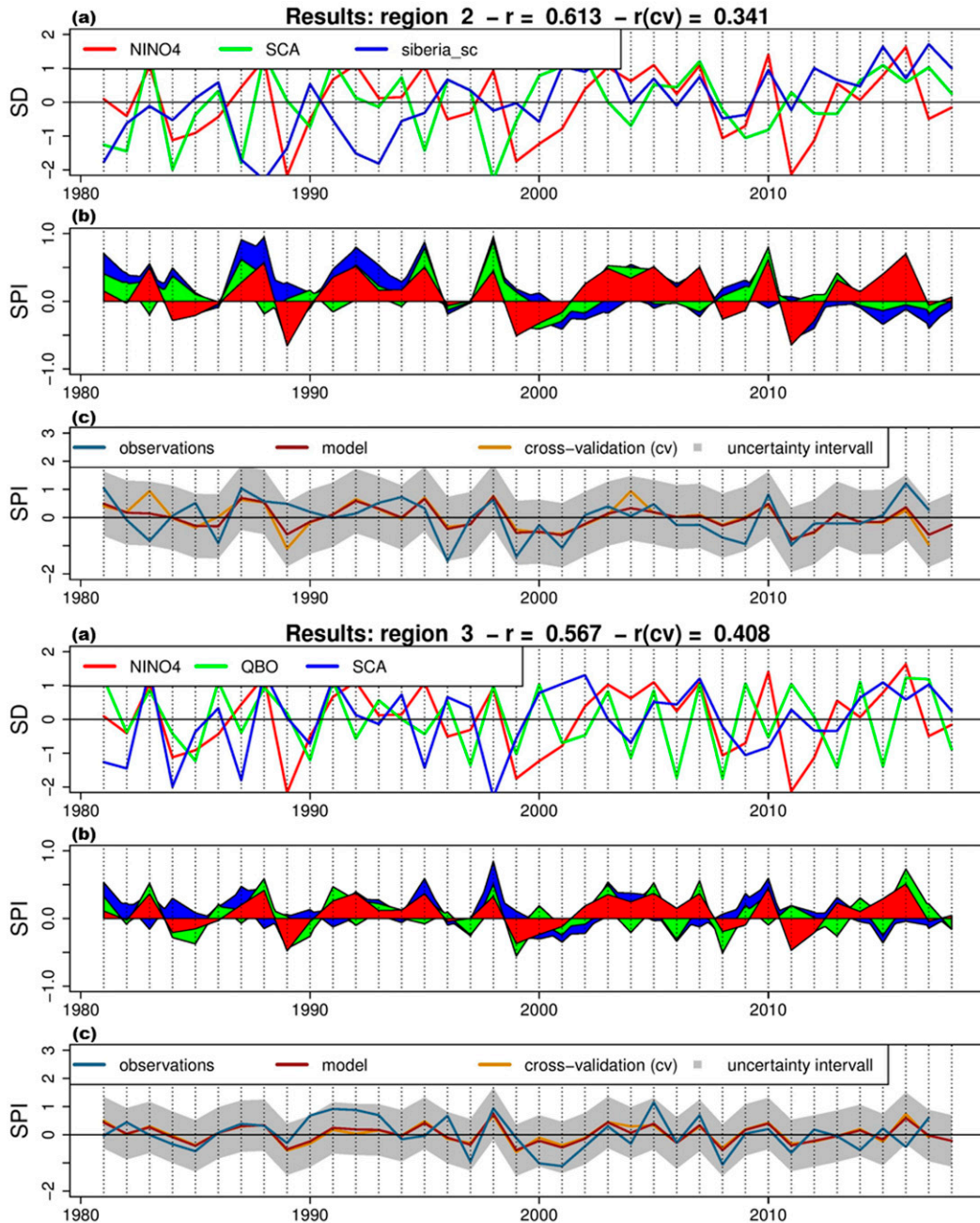
Fig. 2. Hindcast results of the statistical model for regions 2 and 3. (a) Time series of October predictor variables identified by the stepwise predictor selection. (b) Time series of fractional response to selected predictor variables based on the final regression model. (c) Time series of SPI observations as well as hindcast results for the final regression model and the cross-validation procedure. The gray polygon indicates the 90% prediction interval, based on residuals of the cross-validation. Correlations between observations and hindcast results are provided for the final regression and the cross-validation (cv).

b. Atmospheric drivers of precipitation anomalies

1) LARGE-SCALE CIRCULATION FEATURES

The correlation analysis of predictor variables with cold seasonal mean circulation indices indicates a persistence of tropical circulation modes (Fig. 4). Particularly the state of ENSO indices in October shows positive and statistically significant correlations with mean ENSO conditions during subsequent cold season. The same applies to covariates, which are strongly
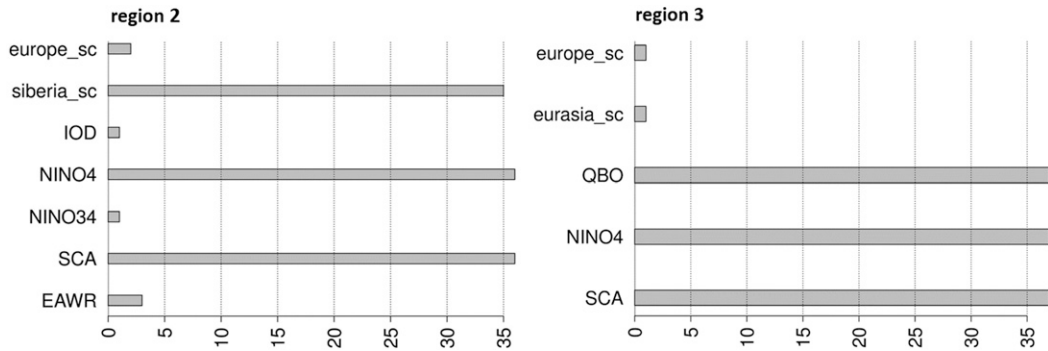
FIG. 3. Predictor selection during cross-validation for regions 2 and 3. Bars indicate the number of linear models, which include the particular covariate (maximum is 37).

correlated with ENSO at a seasonal scale (e.g., the PDO and IOD). Likewise the Scandinavian pattern features a statistically significant persistence for the analyzed period. A persistent behavior of SCA during the cold season and an associated influence on temperature and precipitation anomalies over the Northern Hemisphere have been previously detected. Bueh and Nakamura (2007) show that a mutual influence of the prevailing near-surface circulation and North Atlantic SSTs is likely responsible for the frequent reestablishment of the pattern. Besides the seasonal persistence of some hydroclimatologically relevant circulation features, the
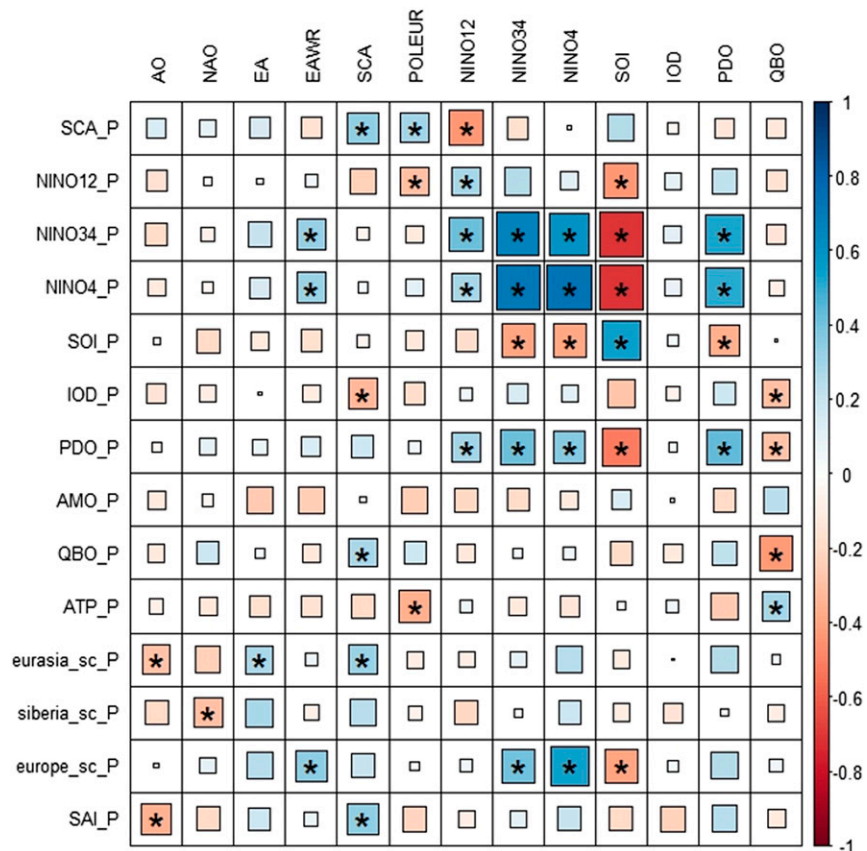
FIG. 4. Pearson correlation matrix of cold seasonal mean circulation indices with the state of selected predictor indices in the preceding October (denoted by _P). The size of squares is proportional to the correlation values. Significant correlations ($\alpha = 0.1$) are marked with an asterisk (*).
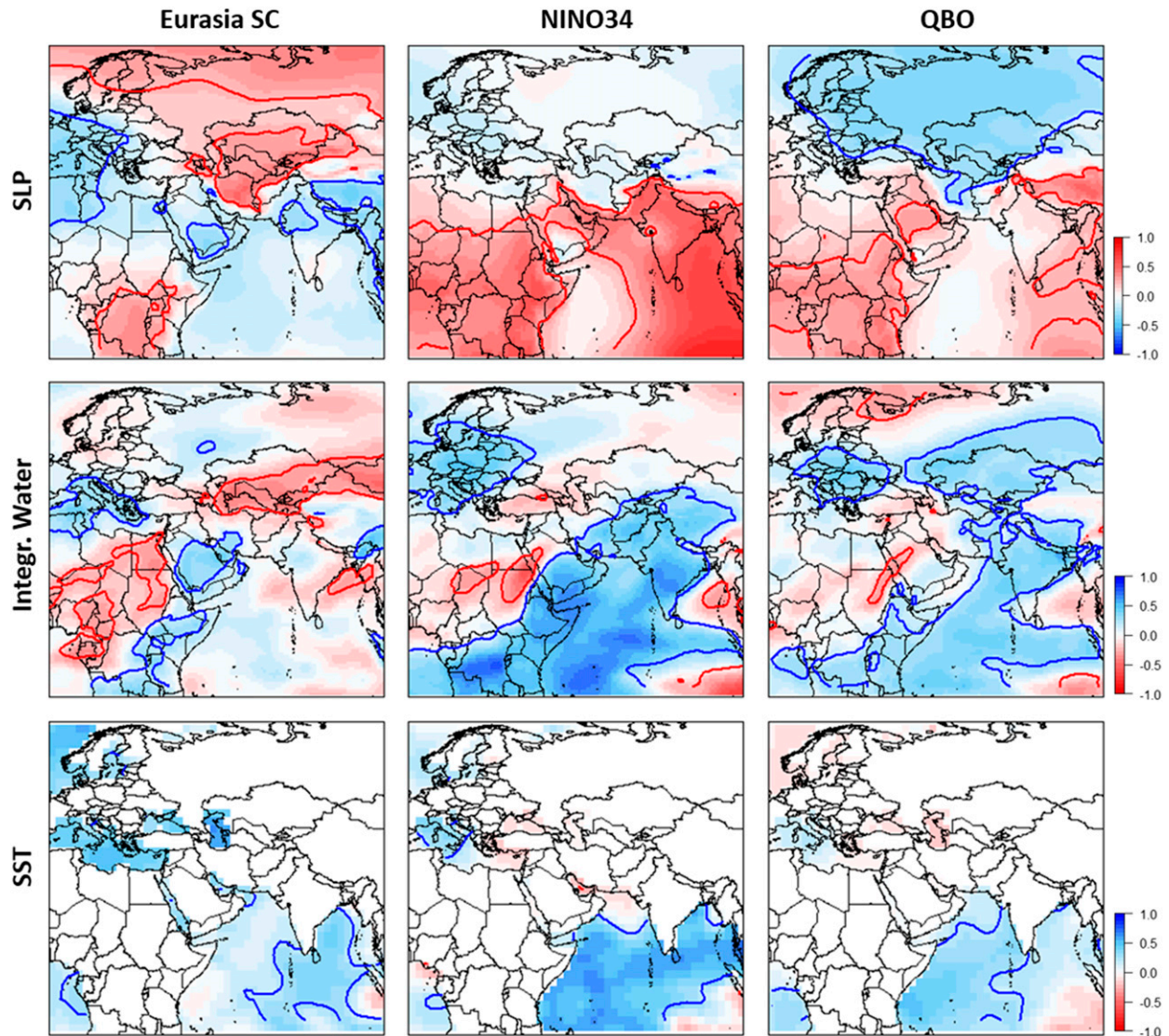
FIG. 5. Pearson correlation maps of cold season mean sea level pressure (SLP), vertically integrated moisture, and sea surface temperature (SST) with Eurasian snow cover extent, the Niño-3.4 index and the QBO index in the preceding October. Bold contour lines indicate the limit of statistically significant correlations ($\alpha = 0.1$). Note that the color scale for SLP is reversed.

correlation matrix indicates a dynamic forcing of westerly circulation modes by snow cover anomalies over Eurasia. In agreement with previous studies (Cohen and Jones 2011; Allen and Zender 2011), negative and partially significant correlations are detected between snow cover anomalies over Eurasia and Siberia in October and the state of the Arctic and North Atlantic Oscillation during the following cold season. Notably, snow cover variations over Europe show a strong positive relationship with the east Atlantic/western Russia pattern in winter, which might indicate a dynamic effect of longitudinal snow cover gradients on the formation of stationary Rossby wave tracks. Further, QBO in

October shows a positive, although nonsignificant, correlation with NAO during winter, which suggests a moderate influence of QBO on westerly circulation characteristics via its effect on the strength and stability of the polar vortex (Boer and Hamilton 2008).

Figure 5 depicts the correlation maps of October Eurasian snow cover, ENSO, and QBO with mean fields of sea level pressure, vertically integrated moisture, and sea surface temperature over Eurasia and the Indian Ocean during the winter season (December–February). Correlation fields for the extended cold season (November–March) feature a similar picture. However results for the latter are less significant (not shown). The

correlation maps indicate a significant influence of snow cover variations on the large-scale circulation over Eurasia. Positive correlations of October snow cover with mean cold seasonal SLP are evident for large parts of northern Eurasia and particularly for central Asia. The zone of positive correlations is sharply bordered by the mountain barriers of Tien Shan, Pamir, and Hindukush. The influence of Siberian snow cover on the large-scale circulation over Eurasia is particularly pronounced during the late winter months (Kretschmer et al. 2016; Cohen et al. 2014, see also Fig. S2). While November conditions preceded by positive snow cover anomalies are characterized by the formation of high sea level pressure over northern Eurasia, a distinct modification of the westerly circulation characteristics is only apparent during January and February. Composite maps of the zonal winds at the 500- and 200-hPa levels (Fig. S2) are clearly similar to the negative state of AO/NAO in late winter and indicate a northward shift of the westerly jet stream over central Asia. The correlation between QBO in October and cold seasonal SLP shows a reversed spatial pattern with significant negative relationships over northern Eurasia. For both Eurasian snow cover and QBO, a significant correlation with the seasonal mean atmospheric moisture content is detected for the central Asian domain.

While snow cover–related indices and QBO significantly influence the prevailing circulation features over the westerly dominated parts of the Eurasian continent, ENSO indices show the strongest correlations with SLP anomalies over the Indian Ocean. El Niño events are typically associated with persistent positive anomalies of SLP over the Indian subcontinent, which increases the tropical moisture supply into central Asia and partly explains the positive correlations with the seasonal mean moisture content (Fig. 5). Besides their influence on large-scale pressure anomalies El Niño events are accompanied by an increase of SSTs over the western Indian Ocean (Fig. 5). This most likely leads to an increased moisture supply due to the amplification of evapotranspiration and thus certainly improves the predictive skill of ENSO related indices.

The EOF analysis of 500-hPa geopotential height (GPH) and vertically integrated moisture for the Eurasian domain (0°–90°E, 20°–70°N) suggests a clear separation of the circulation variability over central Asia into tropical and extratropical modes (Fig. 6). The explained variance of the three major modes of 500-hPa GPH variability amounts to 0.79. The first pattern features a pressure gradient between northern and southern parts of the target domain and clearly resembles the AO/NAO (Fig. 6a). The correlation

of the EOF1 scores with the seasonal mean AO index amounts to $r = 0.72$ (Fig. 6b). Strong negative correlations are detected for the cold seasonal scores of EOF1 with preceding snow cover anomalies over the Eurasian continent, indicating an influence of Eurasian snow cover anomalies in autumn on the westerly circulation characteristics over the central Asian domain (Fig. 6c). In contrast, EOF2 and particularly EOF3 show clear centers of action over the Indian subcontinent and strong pressure gradients over central Asia. Their scores significantly correlate with simultaneous and lagged ENSO indices (Figs. 6a,b). Especially the negative phase of EOF3 features positive GPH anomalies and thus an anticyclonic circulation over the Indian Ocean, which results in an enhanced southwesterly flow during El Niño events. During the negative phase of EOF3, negative GPH anomalies are apparent over the Indian subcontinent, while positive anomalies occur over central Asia. The significantly negative relationship of EOF3 scores with ENSO indices might indicate a dynamic stimulation of a Rossby ridge during La Niña events, as proposed by Barlow et al. (2002).

The EOF loadings of vertically integrated moisture fields feature similar characteristics and likewise separate the circulation variability over the Eurasian domain into a westerly and a tropical portion (Fig. 6a). As for geopotential height, the first mode of variability is characterized by a latitudinal gradient with positive loadings north of the major mountain barriers of Pamir and Tien Shan. Significant correlations are detected with the simultaneous AO index as well as with preceding snow cover anomalies, indicating a dynamic forcing of the Arctic Oscillation by Eurasian snow cover and a consequential modification of moisture fluxes into central Asia. EOF2 is characterized by a pronounced center of action over the Indian subcontinent and the southern parts of central Asia. The EOF2 scores are strongly negatively correlated with simultaneous and lagged ENSO indices, which indicates an intensification of tropical moisture fluxes into central Asia during the ENSO warm phase.

Summarizing, the analysis of large-scale circulation indices, ERA-Interim pressure and moisture fields, and the EOF analysis shows that the major features of the seasonal mean circulation over central Asia can be partitioned into tropical and extratropical modes. A certain degree of predictability has been identified for both fractions of the large-scale circulation, although the strength of statistical relationships is in general larger for tropical modes. These are particularly driven by seasonally persistent variations of ENSO. Westerly circulation features are influenced by deviating boundary conditions,
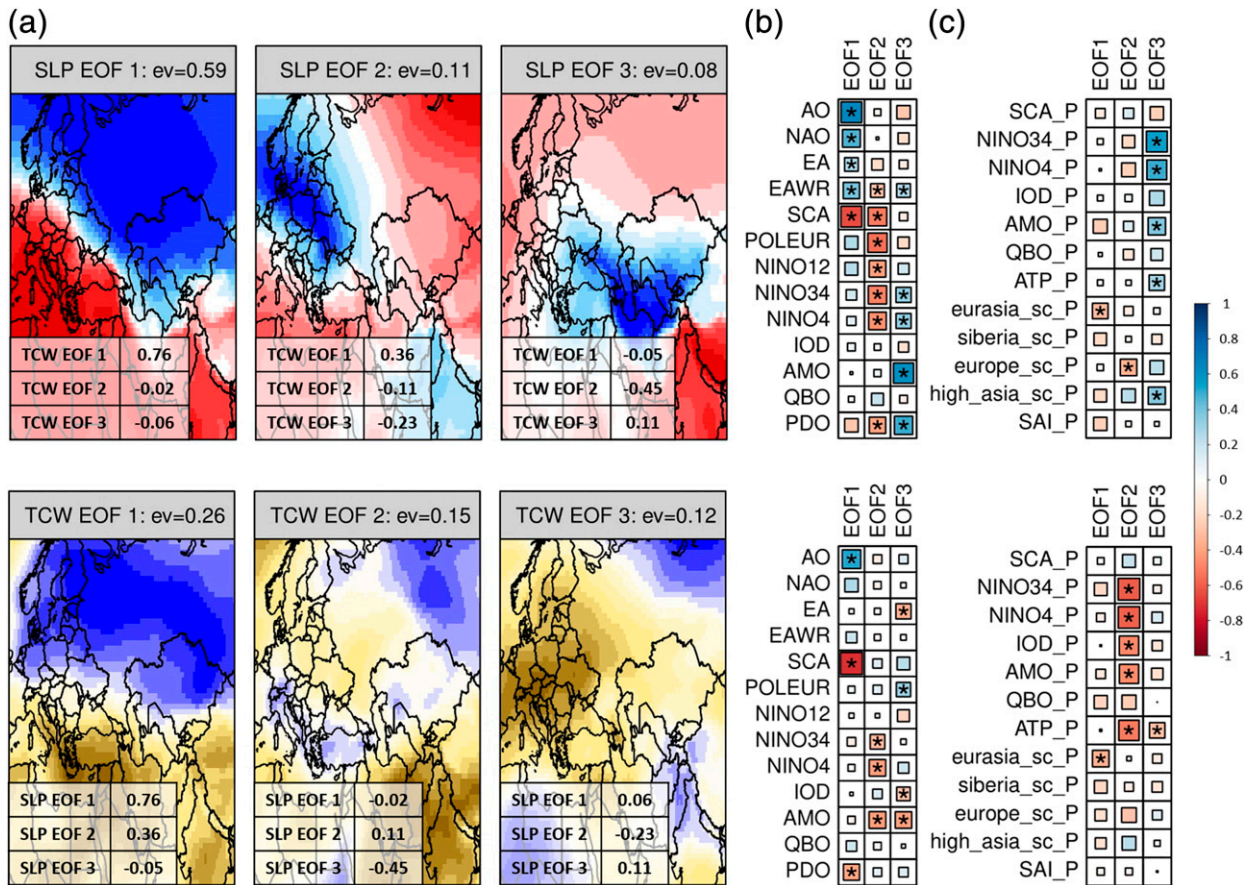
FIG. 6. (a) Spatial distribution of EOF loadings for the major three modes of variability of (top) SLP and (bottom) total column water content (TCW) for the period 1979–2016. The eigenvalues are indicated for each EOF and the correlations between SLP EOF scores and TCW EOF are depicted. (b) Correlations of EOF scores with simultaneous mean seasonal circulation indices. (c) Correlations of EOF scores with selected predictor variables in the preceding October (_P). The size of squares is proportional to the correlation values. Significant correlations ($\alpha = 0.1$) are marked with an asterisk (*).

particularly by snow cover variations over the Eurasian continent, and feature a strong intraseasonal variability.

2) WEATHER TYPE FREQUENCIES

In Part I we established an automatic weather type classification for central Asia. Eight weather types were identified and analyzed with regard to their prevailing pressure patterns and moisture fluxes over Eurasia, their characteristic near-surface climate conditions over central Asia, and their tropical and extratropical drivers. In Fig. 7, the mean 500-hPa geopotential height field as well as the fields of GPH anomalies are depicted and the corresponding vertical integrated moisture fluxes are illustrated for each WT. Precipitation anomalies are shown (normalized by the cold season 6-hourly mean) as well as correlations of WT frequencies with simultaneous variations of selected teleconnection indices. Particularly, WTs 3, 7, and 8 feature strongly positive precipitation anomalies, which are associated with

the formation of a Rossby trough over central Asia (T[KAZ], T[CA]), a southward shift of the frontal jet stream, and a consequential intensification of westerly moisture fluxes over central Asia. The monthly frequencies of those WTs show positive (and partly significant) correlations with the simultaneous east Atlantic/western Russia pattern and the AO/NAO, indicating that the superposition of those circulation modes triggers the formation of a Rossby trough over central Asia and the successional positive precipitation anomalies. On the contrary anticyclonic anomalies due to the formation of a Rossby ridge over central Asia (WT1, WT2, and WT4/R[CA], R[KAZ]) result in a northward shift of westerly moisture fluxes and lead to negative precipitation anomalies. In general, dry WTs show negative (although not always significant) relationships with AO/NAO and EA/WR at a monthly scale. WT5 and WT6 are characterized by a strong meridional flow and a latitudinal precipitation gradient over central Asia. These WTs are
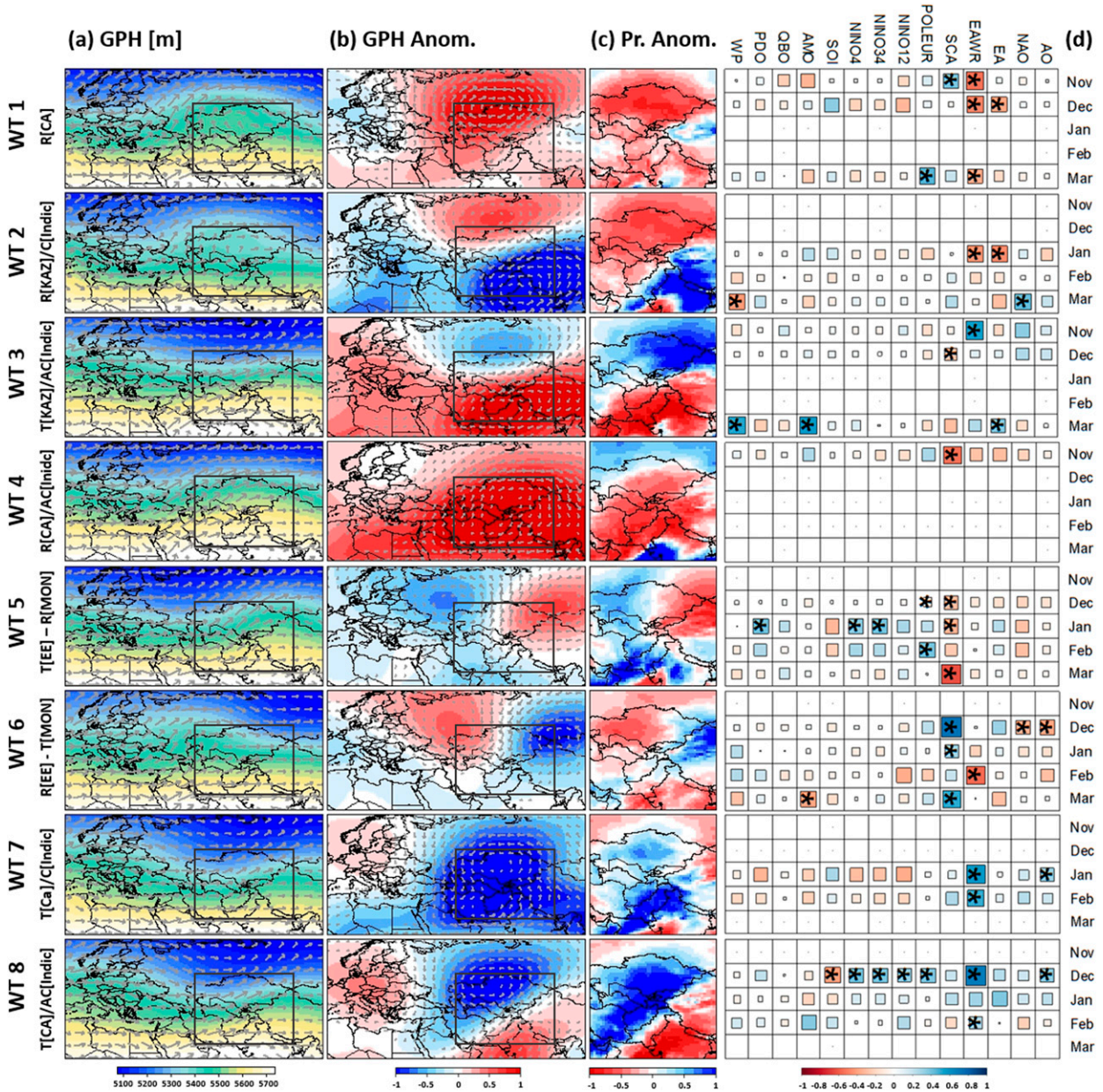
FIG. 7. Major WT characteristics. (a) Mean geopotential height and vertically integrated moisture fluxes over Eurasia. The box displays the region used for the WT classification. (b) Mean GPH anomalies and anomalies of moisture fluxes (standard deviations). (c) Mean anomalies of 6-hourly precipitation anomalies (indicated as a proportion on the cold seasonal mean). (d) Spearman rank correlation between the monthly state of contemporaneous teleconnection indices and the corresponding frequencies of WTs. The size of squares is proportional to the correlation values. Significant correlations are marked with an asterisk (*); $\alpha = 0.1$. Correlations are only depicted if the monthly mean relative WT frequency exceeds 10%. Acronyms indicate the major features (and their centers of action) for each WT: Rossby ridge (R), Rossby trough (T), anticyclonic anomaly (AC), cyclonic anomaly (C), central Asia (CA), Kazakhstan (KAZ), Mongolia (MON), Eastern Europe (EE), and the Indian Ocean and Indian subcontinent (Indic).

strongly related to variations of the Scandinavian pattern and typically occur during negative NAO conditions.

Besides westerly circulation modes, WTs feature pressure anomalies over the Indian Ocean that modulate the southwesterly flow over central Asia and the advection of moist tropical air masses into the target domain. Intensified southwesterly winds are related to the formation of an anticyclonic circulation over the Indian Ocean, which is frequently developed during the ENSO warm phase, and lead to moist conditions in the entire domain
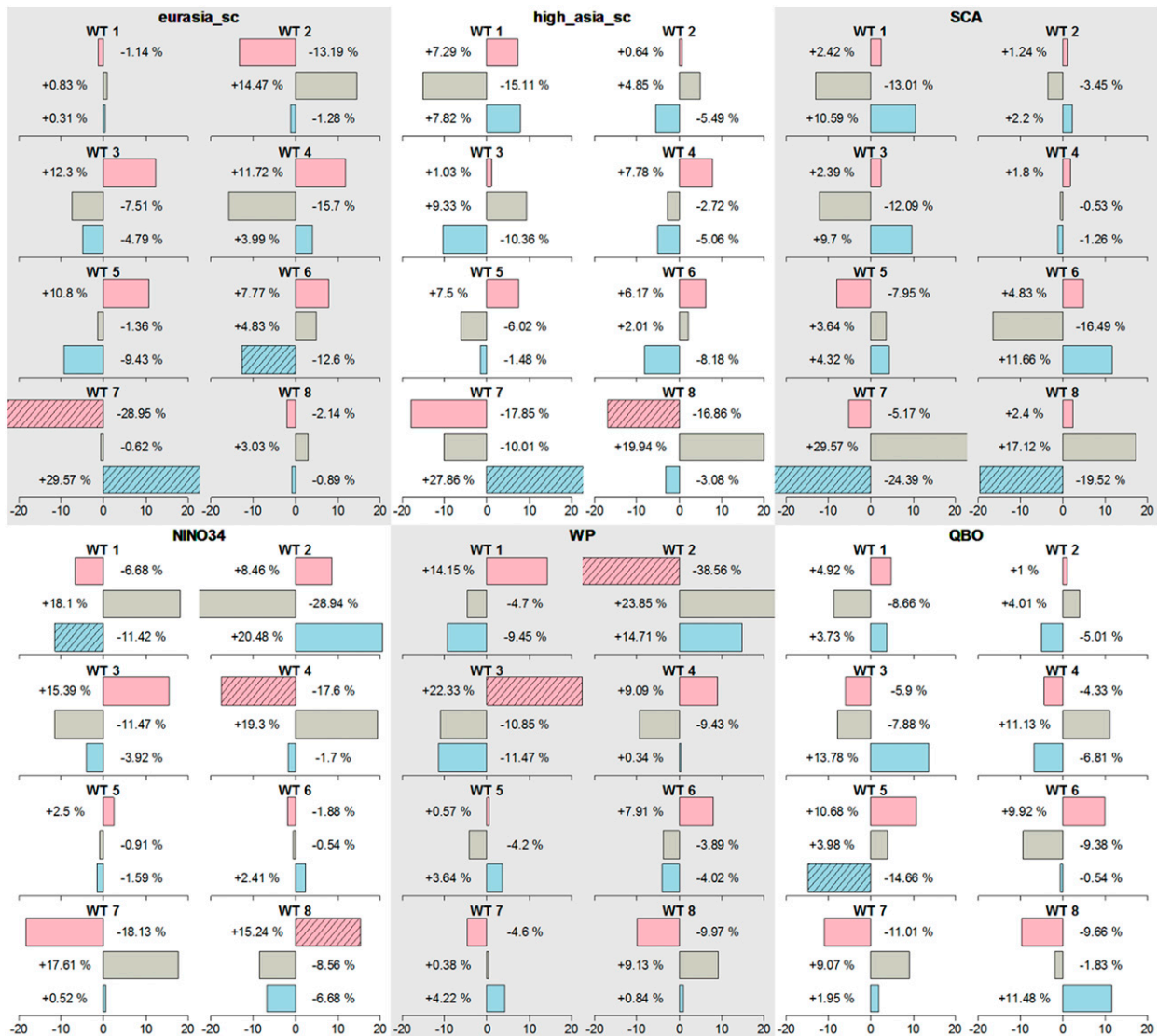
FIG. 8. Influence of predictor variables on the seasonal frequency of WTs. Data are divided into seasons representing rather negative (defined as the 0%–33% quantile; blue bars), normal (33%–66% quantile; gray bars), and positive states (66%–100% quantile; red bars) of the considered index. The mean seasonal WT frequency anomalies (%) during subsequent cold season (November–March) are depicted. Statistically significant deviations from the overall frequency mean (t test; $\alpha = 0.1$) are marked (striped).

(WT6, WT8/AC[Indic]). On the contrary, reduced southwesterlies due to the formation of a low pressure cell and a cyclonic circulation over the Indian Ocean during the ENSO cold phase (WT2, WT7/C[Indic]) provoke drier conditions. Weather types have been shown to represent a superposition and regional manifestation of Euro/Atlantic Rossby waves and pressure anomalies over the Indian Ocean. Both drivers simultaneously modify the synoptic circulation over central Asia.

To quantify the influence of selected predictors of the statistical forecast model on the regional circulation and associated precipitation anomalies over central Asia,

quantile-based bar plots illustrating the anomalies of mean WT frequencies preceded by the 0%–33%, 33%–66%, and 66%–100% quantiles of selected covariates are shown in Fig. 8. Particularly for moist WTs, which are characterized by positive relationships with simultaneous variations of NAO/AO and EA/WR at a monthly scale, a statistically significant influence of snow cover–related predictors is detected. The seasonal mean frequency of WT7 (T[CA]/C[Indic]) is significantly increased in cold seasons preceded by negative snow cover anomalies in October (+29.6%, 0%–33% quantile) and significantly reduced if snow cover in October is above the

66% quantile (−28.9%). For WT 8 (T[CA]/AC[Indic]), which resembles WT7 in terms of GPH variations over northern Eurasia, no statistically significant link with Eurasian snow cover in October is detected, although significantly reduced frequencies preceded by positive anomalies of the snow cover extent over High Asia are observed. Frequencies of WT5 and WT6, which show an increased frequency during the negative phase of AO/NAO, feature a reversed relationship with snow cover–related predictors. Thus there is evidence that the formation of a planetary trough over central Asia, a prominent synoptic feature of the positive AO/NAO (WT3, WT7, and WT8) associated with moisture convergence and positive precipitation anomalies, is partly triggered by reduced snow cover rates over Eurasia in October and a consequential long-lasting modification of the hemispheric circulation in subsequent winter. The dynamical mechanism linking enhanced Eurasian snow cover with an increased strength of the Siberian high, a weakening of the polar vortex, and eventually a negative manifestation of the Arctic Oscillation (Cohen and Entekhabi 1999; Cohen and Jones 2011) might explain the significant correlation between WT frequencies and snow cover variations. Strong relationships for WT7 and WT8 frequencies are further detected with the October state of the Scandinavian pattern. Both WTs show a reduced frequency (−24.3%, −19.5%) preceded by negative SCA indices, which might point to a general tendency toward a stronger meridional flow (i.e., a seasonal persistence of SCA). For example, Bueh and Nakamura (2007) show that SCA is characterized by a stationary behavior and a frequent reestablishment, which leads to a modification of temperature and precipitation patterns at the seasonal scale. Gastineau et al. (2017) and Bueh and Nakamura (2007) further illustrate that snow cover variations over Eurasia are driven by SCA and its downstream wave tracks to a large extent. This suggests an indirect predictive skill of SCA via its influence on the Siberian snowfall, the formation of characteristic Northern Hemispheric wave patterns, and a subsequent modification of the tropospheric and stratospheric dynamics. However the large-scale processes linking SCA in October with WT frequencies in subsequent winter are not fully understood and the robustness of the correlations needs further clarification.

In contrast to AO and SCA, the ENSO circulation is usually regarded as seasonally persistent [see section 3b(1)]. During the ENSO warm phase (El Niño) positive GPH anomalies and thus an anticyclonic circulation anomaly prevail over the Indian Ocean and northern India, resulting in southwesterly winds over Iran and Afghanistan and an advection of tropical moisture from the Red Sea and the Arabian Gulf into central Asia (Fig. 7). Particularly the frequencies of WTs 7 and 8 are significantly influenced by ENSO conditions in previous October. WT7, featuring a cyclonic circulation over the Indian subcontinent (C[Indic]) and a reduced advection of tropical moisture into central Asia, shows a significantly reduced frequency (−18.1%), while its counterpart WT8 (AC[Indic]), which is characterized by strong southwesterly moisture fluxes and highest precipitation amounts, occurs significantly more often (15.2%) during and after El Niño events. A negative influence of ENSO is further evident for the seasonal frequencies of the dry WT4 (R[CA]), which might, in accordance with the EOF analysis provided above, indicate a stimulation of a planetary ridge over central Asia and associated dry conditions during La Niña events (see also Barlow et al. 2002). Besides of their influence on large-scale GPH and circulation anomalies, El Niño events are accompanied by an increase of SSTs over the western Indian Ocean (Fig. 5), which leads to a pronounced WT internal influence of ENSO with higher moisture supply during ENSO events for all WTs (Part I).

Previous studies suggested a link between rising sea surface temperature in the Indo-Pacific warm pool (WP) and prevailing precipitation trends over central Asia. The WP is strongly anticorrelated with ENSO, but features a pronounced positive trend during recent decades (Barlow and Hoell 2015; Barlow et al. 2002; Hoell et al. 2017). However, an additional forecast skill of the WP could not be confirmed in our analysis (see section 3a). Significant deviations of positive and negative warm pool anomalies are detected for frequencies of WT2 and WT3 only. This is inconsistent with the observed relationships with ENSO and might be a statistical artifact due to a common trend. An ENSO independent influence of the WP on the WT composition over central Asia, as supposed by Barlow and Hoell (2015), is not clearly verified. Likewise, no clear influence of the October state of QBO on WT frequencies in subsequent cold season is detected. The correlation with mean sea level pressure in winter (Fig. 5), however, indicates that the positive QBO is associated with negative pressure anomalies over northern Eurasia and central Asia. Slight but not significant positive correlations of the QBO index with the cold seasonal AO and NAO indices are illustrated in Fig. 4. This might indicate a general increase of westerly moisture fluxes during the positive phase of QBO (Marshall and Scaife 2009; Boer and Hamilton 2008), resulting in enhanced seasonal precipitation amounts in central Asia. However, a significant positive relationship between QBO and ENSO [as observed by Yuan et al. (2014); see also Fig. S1 in the supplemental material of this paper] impedes the identification of an independent QBO signal. Therefore, a distinct modification of the regional circulation due to QBO variations remains ambiguous.

4. Summary and discussion

Cold season (November–March) precipitation anomalies have a strong impact on the rural economies of the central Asian countries and robust seasonal forecasts are required in order to enable an adaption to anomalous climate conditions and to implement an application-oriented decision support system in this climatically vulnerable region. Hence there exists demand for simple, user-friendly and computationally efficient tools, which allow a robust forecast of cold seasonal precipitation.

By means of a multivariate linear regression approach including a stepwise predictor selection procedure, moderate forecast skills could be achieved for two subregions covering Uzbekistan, Kyrgyzstan, Tajikistan, and southern Kazakhstan (subregion 2) and Iran, Afghanistan, and northern Pakistan (subregion 3). Cross-validated correlations of observed and predicted cold season precipitation sums in preceding October reach up to 0.34 and 0.41, respectively. ENSO and the Eurasian snow cover extent in October were identified as important predictor variables. The Scandinavian pattern and the quasi-biennial oscillation were found to further improve the statistical forecast skill.

To confirm the statistical relationships and to identify the large-scale and synoptic atmospheric mechanisms resulting in a predictive potential of the considered covariates, a systematic analysis of the cold season climate in central Asia has been conducted at different spatial scales. Results suggest that moist conditions are associated with the persistent regional manifestation of El Niño, which provokes an anticyclonic anomaly over northern India and an enhanced advection of moisture from the Arabian Gulf and the Red Sea. Further, positive anomalies of sea surface temperatures over the western Indian Ocean lead to an increase of evapotranspiration and enhanced moisture supply during El Niño events. Besides ENSO, variations of Northern Hemispheric circulation modes have been shown to propagate into central Asia. Particularly the simultaneous positive manifestation of the Arctic Oscillation and the east Atlantic/western Russia patterns stimulates WTs associated with a Rossby trough over central Asia and a consequential intensification of westerly moisture fluxes.

The Eurasian snow cover extent in October has been shown to influence the regional circulation over Eurasia due to cascading processes at different spatial scales. As previously reported (Handorf et al. 2015; Brands et al. 2012; Cohen and Jones 2011; Cohen and Entekhabi 1999; Nakamura et al. 2015), the winter state of the Arctic Oscillation is affected by snow anomalies over Eurasia during preceding autumn. Positive anomalies

provoke a negative AO via an intensification of the Siberian high and a weakening of the stratospheric polar vortex and vice versa. At a regional scale, the positive state of AO/NAO during winter season favors the formation of a stationary Rossby trough over central Asia, which is associated with strongly positive precipitation anomalies, whereas the negative AO state favors dry conditions.

Some studies indicate that snow cover variations over Eurasia not only influence the interannual variability of the near-surface climate, but also explain observed changes in temperature and precipitation during recent decades. Cohen et al. (2012) explain observed negative temperature trends over Eurasia after 1988 by means of a negative shift of the Arctic Oscillation after the mid-1990s, which is shown to be directly linked with enhanced snow cover over Eurasia. In Part I of the presented study, we show that an observed drying tendency over most parts of central Asia after 1979 can be partially explained a modified WT composition. Although the magnitude of precipitation trends is underestimated, the spatial pattern, with slight positive precipitation trends over the Tien Shan and strongly negative trends in the south of the target domain, is well reproduced by the WT-based reconstruction of seasonal precipitation amounts (Part I). Particularly the frequency of the moist WT7, which is highly positively correlated with the contemporaneous AO, shows a significant negative trend (Part I). This suggests that negative precipitation trends over central Asia are at least partially triggered by increasing Eurasian snow cover and the corresponding AO phase shift in the 1990s.

In general, the pronounced climatic changes in the Arctic, with temperature trends exceeding double the global mean (Screen and Simmonds 2010; Serreze and Francis 2006; Johannessen et al. 2016), have been suggested to strongly influence the snow coverage over the Eurasian continent and the climate of the midlatitudes. Liu et al. (2012) demonstrate that sea ice variations in the Arctic in summer and autumn influence the snow cover extent over Eurasia, particularly due to increased evapotranspiration during ice free periods. Thus, the recent expansion of autumn snow cover over Eurasia and the consequential negative shift of AO might be interpreted as a climate change signal triggered by reduced sea ice extent. Various studies argue that the Arctic amplification and the sea ice loss in the Barents Sea lead to a decreased thermal gradient in the polar regions and thus reduces the atmospheric baroclinity, which drives the westerly jet stream (Cohen et al. 2012; Kretschmer et al. 2016; Gao et al. 2015; Overland 2016). As a consequence, wavier jet stream conditions

(resembling the negative AO), associated with atmospheric blocking or cold air outbreaks in the midlatitudes, become more likely (Barnes et al. 2017; Woollings et al. 2014; García-Herrera and Barriopedro 2006). Di Capua and Coumou (2016) show that the frequency of wavy jet stream conditions during autumn and winter features a significant positive trend after 1979. The formation of planetary wave tracks and associated Northern Hemispheric pressure and humidity patterns have been suggested to strongly influence sea ice conditions in the Arctic (Mann et al. 2017; Li and Wang 2013). Likewise, results by Nakamura et al. (2015) and Handorf et al. (2015) indicate that the winter state of AO is partially triggered by sea ice variations in the Arctic Ocean. This suggests that global warming provokes an increased frequency of extreme weather conditions at the regional scale. Since dry conditions over central Asia are shown to be related to the negative AO state and the associated planetary wave tracks, global warming might lead to an increased drought risk. However, due to a low signal-to-noise ratio in the westerly dominated midlatitudes, the derivation of robust climate change scenarios, especially with regard to hydroclimatic extremes, remains challenging (Chen et al. 2016; Overland 2016; Woollings et al. 2014).

Our study quantifies the statistical relationships of hydroclimatic variations in central Asia with contemporaneous and lagged teleconnection indices by means of a multivariate linear analysis and provides an overview of relevant large-scale and synoptic mechanisms, allowing forecasting of anomalous precipitation amounts during the boreal cold season. Recent studies based on dynamical forecast models for longer periods, however, observed a temporally variant skill of seasonal climate predictions, particularly for the North Atlantic domain (Weisheimer et al. 2017), which points toward nonstationarity of statistical relationships and an interaction of tropical and extratropical circulation modes (Scaife et al. 2014). Thus, the analysis of the robustness of the predictor–predictand relationship, particularly with regard to changing circulation characteristics in the context of global warming, as well as the nonlinear interaction of tropical circulation modes and extratropical wave patterns and their combined influence on the central Asian precipitation climate requires further research.

REFERENCES

Adler, R. F., and Coauthors, 2003: The version-2 Global Precipitation Climatology Project (GPCP) monthly precipitation analysis (1979–present). *J. Hydrometeor.*, **4**, 1147–1167, https://doi.org/10.1175/1525-7541(2003)004<1147:TVGPCP>2.0.CO;2.

Agrawala, S., M. Barlow, H. Cullen, and B. Lyon, 2001: The Drought and Humanitarian Crisis in Central and Southwest Asia: A Climate Perspective. International Research Institute for Climate and Society, Special Rep. 01–11, 20 pp., https://academiccommons.columbia.edu/catalog/ac:126309.

Allen, R. J., and C. S. Zender, 2011: Forcing of the Arctic Oscillation by Eurasian snow cover. *J. Climate*, **24**, 6528–6539, https://doi.org/10.1175/2011JCLI4157.1.

Apel, H., and Coauthors, 2018: Statistical forecast of seasonal discharge in Central Asia using observational records: Development of a generic linear modelling tool for operational water resource management. *Hydrol. Earth Syst. Sci.*, **22**, 2225–2254, https://doi.org/10.5194/hess-22-2225-2018.

Balsamo, G., and Coauthors, 2015: ERA-Interim/Land: A global land surface reanalysis data set. *Hydrol. Earth Syst. Sci.*, **19**, 389–407, https://doi.org/10.5194/hess-19-389-2015.

Bao, X., and F. Zhang, 2013: Evaluation of NCEP–CFSR, NCEP–NCAR, ERA-Interim, and ERA-40 reanalysis datasets against independent sounding observations over the Tibetan Plateau. *J. Climate*, **26**, 206–214, https://doi.org/10.1175/JCLI-D-12-00056.1.

Barlow, M. A., and M. K. Tippett, 2008: Variability and predictability of Central Asia river flows: Antecedent winter precipitation and large-scale teleconnections. *J. Hydrometeor.*, **9**, 1334–1349, https://doi.org/10.1175/2008JHM976.1.

——, and A. Hoell, 2015: Drought in the Middle East and Central–Southwest Asia during winter 2013/14 [in "Explaining Extreme Events of 2014 from a Climate Perspective"]. *Bull. Amer. Meteor. Soc.*, **96** (12), S71–S76, https://doi.org/10.1175/BAMS-D-15-00127.1.

——, H. Cullen, and B. Lyon, 2002: Drought in Central and Southwest Asia: La Niña, the warm pool, and Indian Ocean precipitation. *J. Climate*, **15**, 697–700, https://doi.org/10.1175/1520-0442(2002)015<0697:DICASA>2.0.CO;2.

——, B. Zaitchik, S. Paz, E. Black, J. Evans, and A. Hoell, 2016: A review of drought in the Middle East and Southwest Asia. *J. Climate*, **29**, 8547–8574, https://doi.org/10.1175/JCLI-D-13-00692.1.

Barnes, E. A., E. Dunn-Sigouin, G. Masato, and T. Woollings, 2017: Exploring recent trends in Northern Hemisphere blocking. *Geophys. Res. Lett.*, **41**, 638–644, https://doi.org/10.1002/2013GL058745.

Boer, G. J., and K. Hamilton, 2008: QBO influence on extratropical predictive skill. *Climate Dyn.*, **31**, 987–1000, https://doi.org/10.1007/s00382-008-0379-5.

Bothe, O., K. Fraedrich, and X. Zhu, 2012: Precipitation climate of Central Asia and the large-scale atmospheric circulation. *Theor. Appl. Climatol.*, **108**, 345–354, https://doi.org/10.1007/s00704-011-0537-2.

Brands, S., R. Manzanas, J. M. Gutiérrez, and J. Cohen, 2012: Seasonal predictability of wintertime precipitation in Europe using the snow advance index. *J. Climate*, **25**, 4023–4028, https://doi.org/10.1175/JCLI-D-12-00083.1.

Bueh, C., and H. Nakamura, 2007: Scandinavian pattern and its climatic impact. *Quart. J. Roy. Meteor. Soc.*, **133**, 2117–2131, https://doi.org/10.1002/qj.173.

Cassou, C., L. Terray, J. W. Hurrell, and C. Deser, 2004: North Atlantic winter climate regimes: Spatial asymmetry, stationarity with time, and oceanic forcing. *J. Climate*, **17**, 1055–1068, https://doi.org/10.1175/1520-0442(2004)017<1055:NAWCRS>2.0.CO;2.

Chen, H. W., F. Zhang, and R. B. Alley, 2016: The robustness of midlatitude weather pattern changes due to Arctic sea ice loss. *J. Climate*, **29**, 7831–7849, https://doi.org/10.1175/JCLI-D-16-0167.1.

Cohen, J., 1994: Snow cover and climate. *Weather*, **49**, 150–156, https://doi.org/10.1002/j.1477-8696.1994.tb05997.x.

——, and D. Entekhabi, 1999: Eurasian snow cover variability and Northern Hemisphere climate predictability. *Geophys. Res. Lett.*, **26**, 345–348, https://doi.org/10.1029/1998GL900321.

——, and J. Jones, 2011: A new index for more accurate winter predictions. *Geophys. Res. Lett.*, **38**, L21701, https://doi.org/10.1029/2011GL049626.

——, J. C. Furtado, M. A. Barlow, V. A. Alexeev, and J. E. Cherry, 2012: Arctic warming, increasing snow cover and widespread boreal winter cooling. *Environ. Res. Lett.*, **7**, 014007, https://doi.org/10.1088/1748-9326/7/1/014007.

——, ——, J. Jones, M. Barlow, D. Whittleston, and D. Entekhabi, 2014: Linking Siberian snow cover to precursors of stratospheric variability. *J. Climate*, **27**, 5422–5432, https://doi.org/10.1175/JCLI-D-13-00779.1.

Czaja, A., and C. Frankignoul, 2002: Observed impact of Atlantic SST anomalies on the North Atlantic Oscillation. *J. Climate*, **15**, 606–623, https://doi.org/10.1175/1520-0442(2002)015<0606:OIOASA>2.0.CO;2.

Dee, D. P., and Coauthors, 2011: The ERA-Interim reanalysis: Configuration and performance of the data assimilation system. *Quart. J. Roy. Meteor. Soc.*, **137**, 553–597, https://doi.org/10.1002/qj.828.

Di Capua, G. D., and D. Coumou, 2016: Changes in meandering of the Northern Hemisphere circulation. *Environ. Res. Lett.*, **11**, 094028, https://doi.org/10.1088/1748-9326/11/9/094028.

Dixon, S. G., and R. L. Wilby, 2016: Forecasting reservoir inflows using remotely sensed precipitation estimates: A pilot study for the River Naryn, Kyrgyzstan. *Hydrol. Sci. J.*, **61**, 107–122, https://doi.org/10.1080/02626667.2015.1006227.

Estilow, T. W., A. H. Young, and D. A. Robinson, 2015: A long-term Northern Hemisphere snow cover extent data record for climate studies and monitoring. *Earth Syst. Sci. Data*, **7**, 137–142, https://doi.org/10.5194/essd-7-137-2015.

Gao, L., L. Hao, and X. Chen, 2014: Evaluation of ERA-Interim monthly temperature data over the Tibetan Plateau. *J. Mt. Sci.*, **11**, 1154–1168, https://doi.org/10.1007/s11629-014-3013-5.

Gao, Y., and Coauthors, 2015: Arctic sea ice and Eurasian climate: A review. *Adv. Atmos. Sci.*, **32**, 92–114, https://doi.org/10.1007/s00376-014-0009-6.

García-Herrera, R., and D. Barriopedro, 2006: Northern Hemisphere snow cover and atmospheric blocking variability. *J. Geophys. Res.*, **111**, D21104, https://doi.org/10.1029/2005JD006975.

García-Serrano, J., and C. Frankignoul, 2014: Retraction: High predictability of the winter Euro-Atlantic climate from cryospheric variability. *Nat. Geosci.*, **7**, E2, https://doi.org/10.1038/ngeo2164.

Gastineau, G., J. García-Serrano, and C. Frankignoul, 2017: The influence of autumnal Eurasian snow cover on climate and its link with Arctic sea ice cover. *J. Climate*, **30**, 7599–7619, https://doi.org/10.1175/JCLI-D-16-0623.1.

Gerlitz, L., S. Vorogushyn, H. Apel, A. Gafurov, K. Unger-Shayesteh, and B. Merz, 2016: A statistically based seasonal precipitation forecast model with automatic predictor selection and its application to central and south Asia. *Hydrol. Earth Syst. Sci.*, **20**, 4605–4623, https://doi.org/10.5194/hess-20-4605-2016.

——, E. Steirou, C. Schneider, V. Moron, S. Vorogushyn, and B. Merz, 2018: Variability of the cold season climate in central Asia. Part I: Weather types and their tropical and extratropical drivers. *J. Climate*, **31**, 7185–7207, https://doi.org/10.1175/JCLI-D-17-0715.1.

Guttman, N. B., 1998: Comparing the Palmer Drought Index and the Standardized Precipitation Index. *J. Amer. Water Resour. Assoc.*, **34**, 113–121, https://doi.org/10.1111/j.1752-1688.1998.tb05964.x.

Handorf, D., R. Jaiser, K. Dethloff, A. Rinke, and J. Cohen, 2015: Impacts of Arctic sea ice and continental snow cover changes on atmospheric winter teleconnections. *Geophys. Res. Lett.*, **42**, 2367–2377, https://doi.org/10.1002/2015GL063203.

Harris, I., P. D. Jones, T. J. Osborn, and D. H. Lister, 2014: Updated high-resolution grids of monthly climatic observations—The CRU TS3.10 dataset. *Int. J. Climatol.*, **34**, 623–642, https://doi.org/10.1002/joc.3711.

Hennig, C., 2007: Cluster-wise assessment of cluster stability. *Comput. Stat. Data Anal.*, **52**, 258–271, https://doi.org/10.1016/j.csda.2006.11.025.

Hertig, E., and J. Jacobeit, 2011: Predictability of Mediterranean climate variables from oceanic variability. Part II: Statistical models for monthly precipitation and temperature in the Mediterranean area. *Climate Dyn.*, **36**, 825–843, https://doi.org/10.1007/s00382-010-0821-3.

Hoell, A., M. Barlow, F. Cannon, and T. Xu, 2017: Oceanic origins of historical Southwest Asia precipitation during the boreal cold season. *J. Climate*, **30**, 2885–2903, https://doi.org/10.1175/JCLI-D-16-0519.1.

Johannessen, O. M., S. I. Kuzmina, L. P. Bobylev, and M. W. Miles, 2016: Surface air temperature variability and trends in the Arctic: New amplification assessment and regionalisation. *Tellus*, **68A**, 28234, https://doi.org/10.3402/tellusa.v68.28234.

Kalnay, E., and Coauthors, 1996: The NCEP/NCAR 40-Year Reanalysis Project. *Bull. Amer. Meteor. Soc.*, **77**, 437–471, https://doi.org/10.1175/1520-0477(1996)077<0437:TNYRP>2.0.CO;2.

Kretschmer, M., D. Coumou, J. F. Donges, and J. Runge, 2016: Using causal effect networks to analyze different Arctic drivers of midlatitude winter circulation. *J. Climate*, **29**, 4069–4081, https://doi.org/10.1175/JCLI-D-15-0654.1.

Kumar, A., M. Chen, and W. Wang, 2013: Understanding prediction skill of seasonal mean precipitation over the tropics. *J. Climate*, **26**, 5674–5681, https://doi.org/10.1175/JCLI-D-12-00731.1.

Lautze, S., E. Stites, N. Noyumi, and N. Fazalkarim, 2002: Qaht-e-Pool "A Cash Famine": Food security, malnutrition and the political economy of survival: A report from Kabul, Herat and Qandahar, Afghanistan. Overseas Development Institute, 59 pp., http://reliefweb.int/report/afghanistan/qaht-e-pool-cash-famine-food-security-malnutrition-and-political-economy-survival.

Li, F., and H. Wang, 2013: Autumn sea ice cover, winter Northern Hemisphere annular mode, and winter precipitation in Eurasia. *J. Climate*, **26**, 3968–3981, https://doi.org/10.1175/JCLI-D-12-00380.1.

Liu, J., J. A. Curry, H. Wang, M. Song, and R. M. Horton, 2012: Impact of declining Arctic sea ice on winter snowfall. *Proc. Natl. Acad. Sci. USA*, **109**, 4074–4079, https://doi.org/10.1073/pnas.1114910109.

Liu, Z., Y. Liu, S. Wang, X. Yang, L. Wang, M. H. A. Baig, W. Chi, and Z. Wang, 2018: Evaluation of spatial and temporal performances of ERA-Interim precipitation and temperature in mainland China. *J. Climate*, **31**, 4347–4365, https://doi.org/10.1175/JCLI-D-17-0212.1.

Mann, M. E., S. Rahmstorf, K. Kornhuber, B. A. Steinman, S. K. Miller, and D. Coumou, 2017: Influence of anthropogenic climate change on planetary wave resonance and extreme weather events. *Sci. Rep.*, **7**, 45242, https://doi.org/10.1038/srep45242.

Mariotti, A., 2007: How ENSO impacts precipitation in southwest central Asia. *Geophys. Res. Lett.*, **34**, L16706, https://doi.org/10.1029/2007GL030078.

Marshall, A. G., and A. A. Scaife, 2009: Impact of the QBO on surface winter climate. *J. Geophys. Res.*, **114**, D18110, https://doi.org/10.1029/2009JD011737.

Nakamura, T., K. Yamazaki, K. Iwamoto, M. Honda, Y. Miyoshi, Y. Ogawa, and J. Ukita, 2015: A negative phase shift of the winter AO/NAO due to the recent Arctic sea-ice reduction in late autumn. *J. Geophys. Res. Atmos.*, **120**, 3209–3227, https://doi.org/10.1002/2014JD022848.

New, M., M. Hulme, and P. Jones, 1999: Representing twentieth-century space–time climate variability. Part I: Development of a 1961–90 mean monthly terrestrial climatology. *J. Climate*, **12**, 829–856, https://doi.org/10.1175/1520-0442(1999)012<0829:RTCSTC>2.0.CO;2.

Overland, J. E., 2016: A difficult Arctic science issue: Midlatitude weather linkages. *Polar Sci.*, **10**, 210–216, https://doi.org/10.1016/j.polar.2016.04.011.

R Development Core Team, 2008: R: The R Project for Statistical Computing, R Foundation for Statistical Computing. Accessed 17 December 2015, https://www.r-project.org/.

Roghani, R., S. Soltani, and H. Bashari, 2016: Influence of southern oscillation on autumn rainfall in Iran (1951–2011). *Theor. Appl. Climatol.*, **124**, 411–423, https://doi.org/10.1007/S00704-015-1423-0.

Scaife, A. A., and Coauthors, 2014: Skillful long-range prediction of European and North American winters. *Geophys. Res. Lett.*, **41**, 2514–2519, https://doi.org/10.1002/2014GL059637.

Schär, C., L. Vasilina, F. Pertziger, and S. Dirren, 2004: Seasonal runoff forecasting using precipitation from meteorological data assimilation systems. *J. Hydrometeor.*, **5**, 959–973, https://doi.org/10.1175/1525-7541(2004)005<0959:SRFUPF>2.0.CO;2.

Schiemann, R., D. Lüthi, P. L. Vidale, and C. Schär, 2008: The precipitation climate of Central Asia—Intercomparison of observational and numerical data sources in a remote semiarid region. *Int. J. Climatol.*, **28**, 295–314, https://doi.org/10.1002/joc.1532.

Screen, J. A., and I. Simmonds, 2010: The central role of diminishing sea ice in recent Arctic temperature amplification. *Nature*, **464**, 1334–1337, https://doi.org/10.1038/nature09051.

Serreze, M. C., and J. A. Francis, 2006: The Arctic amplification debate. *Climatic Change*, **76**, 241–264, https://doi.org/10.1007/s10584-005-9017-y.

Smith, T. M., and R. W. Reynolds, 2003: Extended reconstruction of global sea surface temperatures based on COADS data (1854–1997). *J. Climate*, **16**, 1495–1510, https://doi.org/10.1175/1520-0442-16.10.1495.

Sutton, R. T., W. A. Norton, and S. P. Jewson, 2000: The North Atlantic Oscillation—What role for the ocean? *Atmos. Sci. Lett.*, **1**, 89–100.

Syed, F. S., F. Giorgi, J. S. Pal, and M. P. King, 2006: Effect of remote forcings on the winter precipitation of central southwest Asia. Part 1: Observations. *Theor. Appl. Climatol.*, **86**, 147–160, https://doi.org/10.1007/s00704-005-0217-1.

Totz, S., E. Tziperman, D. Coumou, K. Pfeiffer, and J. Cohen, 2017: Winter precipitation forecast in the European and Mediterranean regions using cluster analysis. *Geophys. Res. Lett.*, **44**, 12 418–12 426, https://doi.org/10.1002/2017GL075674.

von Storch, H., and F. W. Zwiers, 2002: *Statistical Analysis in Climate Research.* Cambridge University Press, 995 pp.

Wang, A., and X. Zeng, 2012: Evaluation of multireanalysis products with in situ observations over the Tibetan Plateau. *J. Geophys. Res.*, **117**, D05102, https://doi.org/10.1029/2011JD016553.

Weisheimer, A., N. Schaller, C. O'Reilly, D. A. MacLeod, and T. Palmer, 2017: Atmospheric seasonal forecasts of the twentieth century: Multi-decadal variability in predictive skill of the winter North Atlantic Oscillation (NAO) and their potential value for extreme event attribution. *Quart. J. Roy. Meteor. Soc.*, **143**, 917–926, https://doi.org/10.1002/qj.2976.

Woollings, T., B. Harvey, and G. Masato, 2014: Arctic warming, atmospheric blocking and cold European winters in CMIP5 models. *Environ. Res. Lett.*, **9**, 014002, https://doi.org/10.1088/1748-9326/9/1/014002.

Wu, Z., and H. Lin, 2012: Interdecadal variability of the ENSO–North Atlantic Oscillation connection in boreal summer. *Quart. J. Roy. Meteor. Soc.*, **138**, 1668–1675, https://doi.org/10.1002/qj.1889.

Yatagai, A., K. Kamiguchi, O. Arakawa, A. Hamada, N. Yasutomi, and A. Kitoh, 2012: APHRODITE: Constructing a long-term daily gridded precipitation dataset for Asia based on a dense network of rain gauges. *Bull. Amer. Meteor. Soc.*, **93**, 1401–1415, https://doi.org/10.1175/BAMS-D-11-00122.1.